



Experimental and quantum chemical studies on corrosion inhibition performance of pyrazolic derivatives for mild steel in hydrochloric acid medium, correlation between electronic structure and inhibition efficiency

Ismaily Alaoui K.¹, El Hajjaji F.¹, Azaroual M. A.², Taleb M.¹, Chetouani A.^{3,4*}, Hammouti B.³, Abrigach F.³, Khoutoul M.³, Abboud Y.⁵, Aouniti A.³ and Touzani R.³

¹Laboratoire d'Ingénierie des Matériaux, Modélisation et Environnement, Faculté des Sciences Dhar El Mahraz, Université Allal Ben Abdellah, Atlas, Fès, Morocco

²Laboratoire matériaux électrochimie et environnement Kenitra, Morocco

³Laboratoire de Chimie application et Environnement (LCAE-URAC18), Faculté des Sciences, Université Mohammed Premier, Oujda, Morocco

⁴Laboratoire de chimie physique, Centre Régionale des Métiers de l'Education et de Formation "CRMEF", Région de l'Orientale, Oujda, Morocco

⁵Laboratoire de Physico-Chimie des Matériaux Appliqués, Faculté des sciences Ben M'sik, Université Hassan II Mohammedia- Casablanca, Morocco

ABSTRACT

The inhibition of the corrosion of steel in 1 M HCl by pyrazole compounds 5-bromo-N-((3,5-dimethyl-1H-pyrazol-1-yl)pyridine-2-amine (AB8) and 3,5-dibromo-N-((3,5-dimethyl-1H-pyrazol-1-yl)pyridine-2-amine (AB9) has been studied by weight loss, electrochemical polarisation and electrochemical impedance spectroscopy measurements. The results obtained reveal that these compounds are efficient inhibitors. The inhibition efficiency increases with the increase of inhibitor concentration and reached 95 % for AB9 at 10^{-3} M. Potentiodynamic polarisation studies clearly reveal that the presence of all inhibitors does not change the mechanism of hydrogen evolution and that they act mixed inhibitors. The temperature effect on the corrosion behaviour of steel in 1 M HCl without and with the inhibitors at 10^{-3} M was studied in the temperature range from 308-333K, it allows to determine the several thermodynamic parameters. The inhibitors were adsorbed on the steel surface according to the Langmuir adsorption isotherm model. From the adsorption isotherm some thermodynamic data for the adsorption process are calculated and discussed. Geometries optimization of all molecules considered in this study were fully optimized by using gradient corrected DFT with Becke's three-parameter hybrid exchange functional and the Lee-Yang-Parr correlation functional (B3LYP) and with the 6-31G basis. The theoretical studies are to reduce the cost of research and the results obtained for corrosion inhibitors of mild-steel by this inhibitors demonstrated that correlation exists between inhibition efficiency and all parameters quantum chemicals. The directly calculated ionization potential (IP), electron affinity (A), dipole moment (μ), electronegativity (χ), electron affinity (A), global hardness (η), softness (σ), the global electrophilicity (ω), the fraction of electrons transferred (ΔN), are all in good agreement with the available experimental data.

Keywords: pyrazolic; corrosion; inhibition; steel; hydrochloric acid solution, Density functional theory (DFT).

INTRODUCTION

Mild steel is employed widely in most industries in due of low cost and its availability in ease for the fabrication of various reaction vessels such as cooling tower tanks, pipelines, etc. Acid solutions are generally used for the removal of undesirable scale and rust in several industrial processes. Inhibitors are generally used in these processes to control metal dissolution. An important practical application of such phenomena is corrosion inhibition.

Numerous investigations have been performed on the inhibition of iron and iron-based alloy by using of organic compounds [1-4]. Of practical interest in the general field of organic inhibitors are the nature of the chemical bond at the metal surface and an explanation of why these substances often provide such excellent protection when adsorbed. Therefore, they minimise the direct interaction between the metal and corrosive agents. In some cases, the coordination of the inhibitor molecules to the surface is weak, and their presence in the corrosive solutions required maintaining the desired concentration of these agents to the metal surface. As some inhibitor molecules also serve as reducing agents for the copper oxidation products, they must be continuously added to avoid other possible corrosion shape [5-9].

To this subject, in the past few decades numerous investigations were performed using the traditional electrochemical methods. The effect of organic compounds containing heteroatom on the corrosion behaviour of iron and steel in acidic solutions has been well showed to be quite efficient to prevent corrosion and in addition to heterocyclic compounds containing polar groups and π -electrons. The inhibiting action of those organic compounds is usually attributed to interactions with metallic surfaces by adsorption. The polar function is frequently regarded as the reaction centre for the adsorption process establishment, being the adsorption bond strength determined by the electron density and polarizability of the functional group [10-15].

During the past decade, the inhibition of corrosion in acid solutions can be effectuated by the addition of a variety of organic compounds and has been investigated by several workers. The aim of this paper is to study the corrosion behaviour of mild steel in 1M HCl in the presence and absence of the 5-bromo-N-((3,5-dimethyl-1H-pyrazol-1-yl)pyridine-2-amine (AB8) and 3,5-dibromo-N-((3,5-dimethyl-1H-pyrazol-1-yl)pyridine-2-amine (AB9) compounds at 308K. Weight-loss measurements combined with linear potential scan voltammetry (*I-E*) and electrochemical impedance spectroscopy (*EIS*) were performed in order to complete and to compare the results obtained.

The quantum chemical calculations have been widely used to study the reaction mechanisms and to interpret the experimental results as well as to solve chemical ambiguities. This is a useful approach to investigate the mechanisms of reaction in the molecule and its electronic structure level and electronic parameters can be obtained by means of theoretical calculations using the computational methodologies of quantum chemistry [9]. The advancement in methodology and implementations has reached a point where predicted properties of reasonable accuracy can be obtained from density functional theory (DFT) calculations [16]. The geometry of the inhibitor in its ground state, as well as the nature of their molecular orbitals, highest occupied molecular orbital (HOMO) and lowest unoccupied molecular orbital (LUMO) are involved in the properties of activity of inhibitors. The inhibition property of a compound has been often correlated with energy of HOMO, LUMO and HOMO-LUMO gap. The inhibition efficiency of the two inhibitors was studied previously [10; 17].

The objective of this paper is to investigate the dependence of inhibition efficiency of these compounds on theoretical chemical parameters such as the energies of highest occupied molecular orbital (E_{HOMO}) and the lowest unoccupied molecular orbital (E_{LUMO}), the energy difference (ΔE) between E_{HOMO} and E_{LUMO} , dipole moment (μ), electronegativity (χ), electron affinity (A), global hardness (η), softness (σ), ionization potential (I), the global electrophilicity (ω), the fraction of electrons transferred (ΔN) and the total energy (TE). The chemical structures of the compounds studied are given in Fig 1 [18-20].

EXPERIMENTAL SECTION

1.1. Inhibitors

A bidentate pyrazolic compounds **AB8** and **AB9** were synthesized by condensation of the (3,5-dimethyl-1H-pyrazol-1-yl) methanol with appropriate primary amines in reflux acetonitrile for 4 hours and characterized .for **5-bromo-N-((3,5-dimethyl-1H-pyrazol-1-yl)methyl)pyridin-2-amine (AB8)** : Solid; Yield: 20.29%; mp: 148-152 °C. **IR** (KBr, ν (cm^{-1})): 3425(NH); 3263-2926(CH); 1577(C=N); 1500(C=C); 1359(C-N aromatic); 1294(C-N aliphatic); 613(C-Br). **¹H NMR** (300 MHz, CDCl_3) δ ppm : 8.11 (dd, 1H, CH⁽⁶⁾ of pyridine, $J_{\text{H-H}}=6$ Hz) ; 7.73 (dd, 1H, CH⁽³⁾ of pyridine, $J_{\text{H-H}}=3.3$ Hz) ; 5.82 (s, 1H, CH⁽⁴⁾ of pyrazole); 5.65 (d, 2H, N-CH₂-N, $J_{\text{H-H}}=6.6$ Hz) ; 4.48 (s, 1H, NH) ; 2.43 (s , 3H, CH₃⁽⁵⁾ of pyrazole) ; 2.22 (s , 3H, CH₃⁽³⁾ of pyrazole). **¹³C NMR** (75 MHz, CDCl_3) δ ppm:152.94 (C⁽²⁾-NH); 151.81(CH⁽⁶⁾ of pyridine); 146.76 (CH⁽⁴⁾ of pyridine);111.11 (CH⁽³⁾ of pyridine); 105.45 (CH⁽⁴⁾ of pyrazole); 53.76 (N-CH₂-N); 13.19 (CH₃⁽³⁾ of pyrazole); 10.68 (CH₃⁽⁵⁾ of pyrazole). **For 3,5-dibromo-N-((3,5-dimethyl-1H-pyrazol-1-yl)methyl)pyridin-2-amine (AB9)**: Solid; Yield: 63.67%; mp: 156-160 °C. **IR** (KBr, ν (cm^{-1})): 3431(NH); 3263-2916(CH); 1581(C=N); 1504(C=C); 1359(C-N aromatic); 1294(C-N aliphatic); 617(C-Br). **¹H NMR** (300 MHz, CDCl_3) δ ppm : 8.11 (dd, 1H, CH⁽⁶⁾ of pyridine, $J_{\text{H-H}}=5.7$ Hz) ; 7.73 (dd, 1H, CH⁽⁴⁾ of pyridine, $J_{\text{H-H}}=3.6$ Hz); 5.76 (s, 1H, CH⁽⁴⁾ of pyrazole); 5.64 (d, 2H, N-CH₂-N, $J_{\text{H-H}}=6.6$ Hz) ; 4.88 (s, 1H, NH) ; 2.43 (s , 3H, CH₃⁽⁵⁾ of pyrazole) ; 2.22 (s , 3H, CH₃⁽³⁾ of pyrazole). **¹³C NMR** (75 MHz, CDCl_3) δ ppm:

151.81 (CH⁽⁶⁾ of pyridine); 141.92 (CH⁽⁴⁾ of pyridine); 105.44 (CH⁽⁴⁾ of pyrazole); 53.78 (N-CH₂-N); 13.23 (CH₃⁽³⁾ of pyrazole); 11.15 (CH₃⁽⁵⁾ of pyrazole). MS [M⁺] (m/z): calculated 360.05, found 360.73

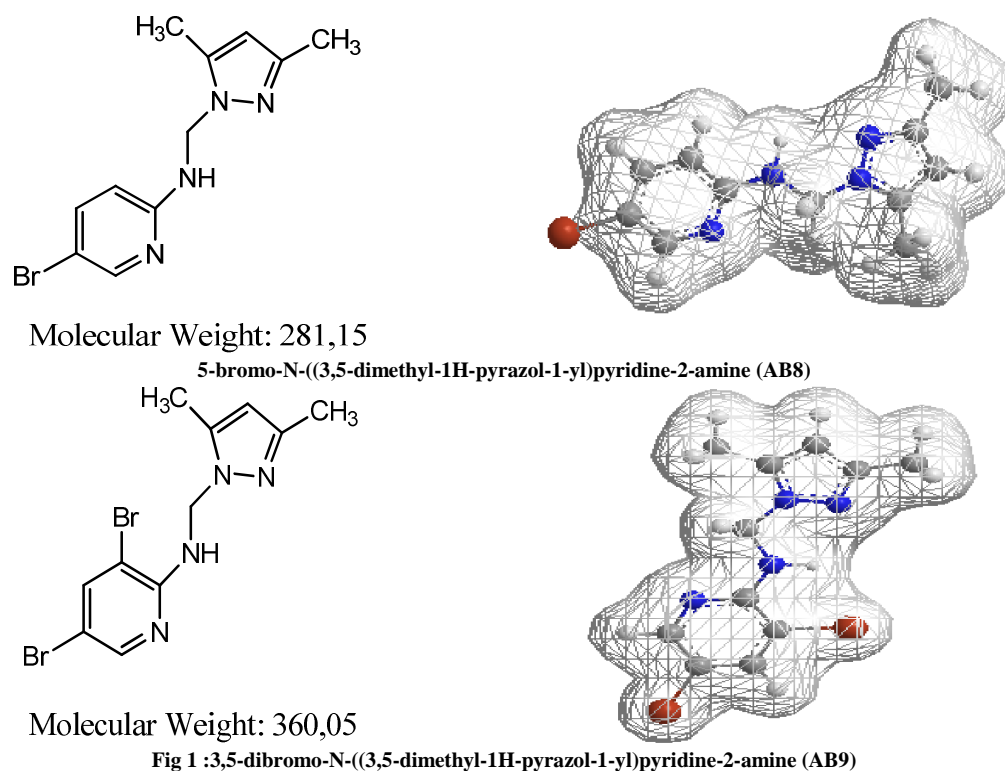


Fig 1 :3,5-dibromo-N-((3,5-dimethyl-1H-pyrazol-1-yl)pyridine-2-amine (AB9)

2.2. Methods and materials

Prior each gravimetric or electrochemical experiment, the surface of the specimens was abraded successively with emery paper. The specimens are then rinsed with acetone and bid stillled water. Weight loss was measured on sheets of steel of 2cm² apparent surface area. The samples were polished successively with different emery paper up 1000 grade, washed with distilled water, degreased and dried before being weighed and immersed in 100 ml of the corrosive medium.

The aggressive solution (1M HCl) was prepared by dilution of analytical-grade 37% HCl with doubly distilled water. All tests were obtained in magnetically stirred and de-aerated solutions. The immersion time for the weight loss measurements was 6 hours at 308K. The chemical composition of mild steel is given in Table 1:

Table 1. The chemical composition of mild steel

%C	%Si	%Mn	%S	%P	%AL	%Fe
0.21	0.38	0.05	0.05	0.09	0.01	99.21

Electrochemical impedance spectroscopy (EIS) and is carried out with a Voltalab PGZ 100 electrochemical system at E_{corr} after immersion in solution. After determination of the steady-state current at a given potential, sine wave voltage (10mV) peak to peak, at frequencies between 100 kHz and 10 mHz is superimposed on the rest potential. Computer programs automatically controls the measurements performed at rest potentials after 30 min of exposure. EIS diagrams are given in the Nyquist representation.

The potentiodynamic current-voltage characteristics are recorded also with a Voltalab PGZ 100, piloted by ordinate, at a scan rate of 1 mV/s. The potential started from cathodic to anodic potential. Before recording each curve, the working electrode is maintained with its free potential of corrosion for 30 min. We used for all electrochemical tests a cell with three electrodes thermostats with double wall (Tacussel Standard CEC/TH). Saturated calomel electrode (SCE) and platinum electrode are used as reference and Auxiliary electrodes, respectively. The working electrode is in form of disc from steel of the surface 1 cm².

2.3. Computational Chemistry

DFT (density functional theory) methods were used in this study. These methods have become very popular in recent years because they can reach exactitude similar to other methods in less time and less expensive from the

computational point of view. In agreement with the DFT results, energy of the funAB8 and AB9ntal state of a polyelectronic system can be expressed through the total electronic density, and in fact, the use of electronic density instead of wave function for calculating the energy constitutes the funAB8 and AB9ntal base of DFT. All calculations were done by GAUSSIAN 03 W software, using the B3LYP functional and a 6-31G* basis set. The B3LYP, a version of DFT method, uses Becke's three-parameter functional (B3) and includes a mixture of HF with DFT exchange terms associated with the gradient corrected correlation functional of Lee, Yang, and Parr (LYP) [18; 21]. The geometry of all species under investigation was determined by optimizing all geometrical variables without any symmetry constraints. Frontier molecular orbital's (*HOMO* and *LUMO*) may be used to predict the adsorption centres of the inhibitor molecule. For the simplest transfer of electrons, adsorption should occur at the part of the molecule where the softness, σ , which is a local property, has the highest value. According to Koopman's theorem [25], the energies of the *HOMO* and the *LUMO* orbitals of the inhibitor molecule are related to the ionization potential, I , and the electron affinity, A , respectively, by the following relations: $I = -E_{HOMO}$ and $A = -E_{LUMO}$. Absolute electronegativity, χ , and absolute hardness, η , of the inhibitor molecule are given by [26]. $\chi = \frac{I + A}{2}$ and $\eta = \frac{I - A}{2}$. The softness is the inverse of the hardness: $\sigma = \frac{1}{\eta}$. The obtained values of χ and η are used to calculate the fraction of electron transferred, ΔN , from the inhibitor to metallic surface

as follow: $\Delta N = \frac{\chi_{Fe} - \chi_{inh}}{2(\eta_{Fe} + \eta_{inh})}$. Where χ_{Fe} and χ_{inh} denote the absolute electronegativity of *Fe* and the inhibitor

molecule, respectively; ρ_{Fe} and ρ_{inh} denote the absolute hardness of *Fe* and the inhibitor molecule, respectively. A theoretical value for the electronegativity of bulk iron was used $\chi_{Fe} = 7$ eV and a global hardness of $\rho_{Fe} = 0$, by assuming that for a metallic bulk $IP = EA$ because they are softer than the neutral metallic atoms.

RESULTS AND DISCUSSION

3.1. Weight loss tests

The effect of addition of 5-bromo-N-((3,5-dimethyl-1H-pyrazol-1-yl)pyridine-2-amine (AB8) and 3,5-dibromo-N-((3,5-dimethyl-1H-pyrazol-1-yl)pyridine-2-amine (AB9) compounds tested at different concentrations on the corrosion of steel in de-aerated 1M HCl solution was studied by weight-loss at 298 °k after 6 hours of immersion period. Inhibition efficiency (E%) were calculated as follows:

$$E\% = \left(1 - \frac{W_{cor}}{W_{cor}^o} \right) \cdot 100 \quad (1)$$

W^o and w are the corrosion rates of steel samples in the absence and presence of the organic compound, respectively.

The results of weight loss of steel in 1M HCl with and without the addition of various concentrations of the compound pyrazolic –type compounds are given in table (2).

The results given in table (2) show that it clear that for each compounds tested, the steel corrosion rate values decrease when the concentration of pyrazolic compounds increases.

The inhibiting action is more pronounced with 5-bromo-N-((3,5-dimethyl-1H-pyrazol-1-yl)pyridine-2-amine (AB8) and 3,5-dibromo-N-((3,5-dimethyl-1H-pyrazol-1-yl)pyridine-2-amine (AB9), and its inhibition efficiency attains the maximum value of 90.6% and 94.6% respectively at the 10^{-3} M. It was shows that the protective properties of such compounds depend upon their ability to reductive corrosion rate and are enhanced at higher electron densities around nitrogen atoms. They reported that the nitrogen atoms is the adsorption centres for their interaction with the metal surface. The all organic compounds, AB8 and AB9, containing electron negative function groups, heterocyclic and π electrons conjugated are good inhibitors. the mesomeric effect or resonance effect in chemistry is a property of substituents or functional groups in a chemical compound. The effect is used in a qualitative way and describes the electron withdrawing or releasing properties of substituents based on relevant resonance structures. The mesomeric effect is negative Bromide atoms (Br) when the substituent is an electron-withdrawing group and the effect is positive (pyridine cycle) when based on resonance and the substituent is an electron releasing group. Effectively, This order is mainly due to the nature of the substituent: the bromide atoms in position 3 and 3,5 for AB8 and AB9 respectively. It's well known that different substituent's on the organic molecule polarize the functional group in a different position and the inhibition efficiency of organic inhibitor containing heteroatom's [6].

Table 2: gravimetric results of steel corrosion in 1M HCl without and with addition of different pyrazolic compounds studied at 308k after 6 hour of immersion period

Inhibitors	Concentrations (M)	W(mg.cm ² .h ⁻¹)	Inhibition Efficiency (%)
1M HCl	0	0.962	----
AB8	5.10 ⁻⁶	0.266	72.3
	10 ⁻⁵	0.252	73.8
	5.10 ⁻⁵	0.206	78.6
	10 ⁻³	0.147	84.7
	5.10 ⁻⁴	0.126	86.9
	10 ⁻³	0.090	90.6
AB9	5.10 ⁻⁶	0.229	76.2
	10 ⁻⁵	0.200	79.2
	5.10 ⁻⁵	0.152	84.2
	10 ⁻³	0.130	86.4
	5.10 ⁻⁴	0.108	88.7
	10 ⁻³	0.052	94.6

We concluded that the inhibition efficiencies of these compounds is understandable from the electron donor properties of Nitrogen atoms in the structure of which one finds a delocalisation π electron between nitrogen atoms who permits therefore reinforced for the interaction.

3.2. Polarization results.

To complete and to compare the results obtained before, the corrosion behaviour of steel, in acid solution with and without inhibitors, was investigated by electrochemical methods. The typical cathodic polarization behaviour of steel 1M HCl in absence and presence of AB8 and AB9 are shown in fig 2. As can be seen from figure, cathodic polarization curves rise to parallel Tafel lines indicating that the hydrogen evolution reaction is activation controlled and the presence of pyrazolic compounds does not affect the mechanism of this process. That means that the inhibition of the hydrogen evolution reaction by pyrazolic investigated occurs by simple adsorption mode and the mechanism is the same without addition of pyrazolic tested [22].

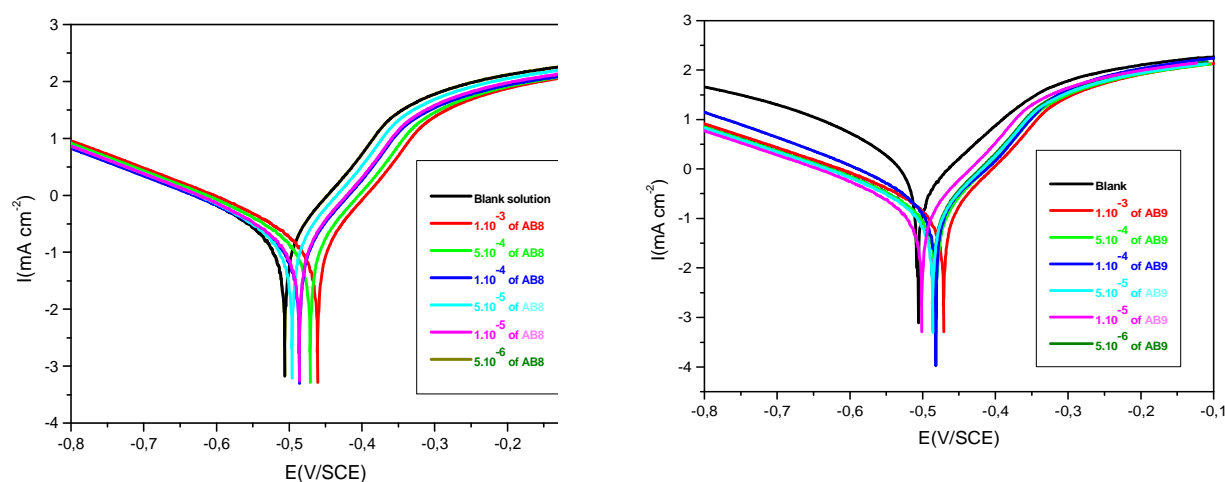


Fig 2 : linear polarisation plots of steel in 1M HCl for various concentrations of AB8 and AB9

Table (3) gives values of corrosion current (I_{cor}), corrosion potential (E_{cor}), cathodic Tafel slope b_c for different compounds organic in 1M HCl for the tested compounds. In the case of polarization method the relation determines the inhibition efficiency ($E\%$), where I_{cor}^o and I_{cor} are the uninhibited and inhibited corrosion current densities, respectively, determined by extrapolation of cathodic Tafel lines to corrosion potential [2; 4].

$$E_I \% = \left(1 - \frac{I_{cor}}{I_{cor}^o}\right) \cdot 100 \quad (2)$$

From results obtained in the Table (3), a decrease of corrosion current densities when the increase of the concentration of the inhibitor was noted. The inhibiting action is more pronounced with AB9 and AB9 and their inhibition efficiency

attains a maximum value of 96% and 94%, respectively, at 10^{-3} M. From the anodic curves we deduce that P1 acts as a mixed-type inhibitor; but AB8 and AB9 acts essentially a cathodic type inhibitor Fig.2.

Table 3: Electrochemical parameters for steel in 1M HCl at various concentrations of AB8, AB9 at 298 K

	Concentration (M)	E_{corr} (mV /SCE)	I_{corr} $\mu\text{A}/\text{cm}^2$	b_a mV/dec	b_c mV/dec	E%
HCl	1M	-521,3	2,1141	173,5	15,8	--
AB8	1.10^{-3}	-462,1	78,4800	169,5	13,8	94
	5.10^{-4}	-493,8	104,6480	167,3	12,9	92
	1.10^{-4}	-418,1	222,3650	164,2	13,7	83
	5.10^{-5}	-500,2	274,6800	163,6	13,4	79
	1.10^{-5}	-485,9	340,0880	163,2	13,9	74
	5.10^{-6}	-469,2	379,3290	162,5	14,2	71
AB9	1.10^{-3}	-470,7	52,3210	169,5	12,6	96
	5.10^{-4}	-476,4	170,0400	167,0	14,7	87
	1.10^{-4}	-480,2	196,2051	166,4	14,2	85
	5.10^{-5}	-482,6	248,5200	185,4	15,2	81
	1.10^{-5}	-501,7	287,7674	172,0	13,2	78
	5.10^{-6}	-488,2	313,9281	187,6	13,4	76

All heterocyclic (pyrazolic and pyridine) of AB8 and AB9 containing nitrogen and electron negative functional groups π electrons in their structure and the conjugated double bands have been proved to perform as very good inhibitors for the corrosion of steel in acidic solution.

3.3. Electrochemical impedance spectroscopy (EIS)

Dielectric spectroscopy (sometimes called impedance spectroscopy), and also known as electrochemical impedance spectroscopy (EIS), measures the dielectric properties of a medium as a function of frequency. It is based on the interaction of an external field with the electric dipole of the sample, often expressed by permittivity.

It is also an experimental method of characterizing electrochemical systems. This technique measures the impedance of a system over a range of frequencies, and therefore the frequency response of the system, including the energy storage and dissipation properties, is revealed. Often, data obtained by EIS is expressed graphically in a Bode plot or a Nyquist plot. Impedance is the opposition to the flow of alternating current (AC) in a complex system. A passive complex electrical system comprises both energy dissipater (resistor) and energy storage (capacitor) elements. If the system is purely resistive, then the opposition to AC or direct current (DC) is simply resistance. Almost any physic-chemical system, such as electrochemical cells, mass-beam oscillators, and even biological tissue possesses energy storage and dissipation properties. EIS examines them. This technique has grown tremendously in stature over the past few years and is now being widely employed in a wide variety of scientific fields such as fuel testing, bimolecular interaction, and microstructure characterization. Often, EIS reveals information about the reaction mechanism of an electrochemical process: different reaction steps will dominate at certain frequencies, and the frequency response shown by EIS can help identify the rate limiting step [23; 24; 25; 26].

The corrosion behaviour of steel in 1M hydrochloric acidic solution, in the absence and presence of the pyrazolic compounds, is also investigated by the EIS at 308 K after 30min of immersion. The charge-transfer resistance (R_t) values are calculated from the difference in impedance at lower and higher frequencies, as suggested. The double layer capacitance (C_{dl}) and the frequency at which the imaginary component of the impedance is maximal ($-Z_{\text{max}}$) are found as represented in equation:

$$C_{dl} = 1/\omega.R_t \quad \text{where } \omega = 2 \pi . f_{\text{max}} \quad (3)$$

The inhibition efficiency got from the charge-transfer resistance is calculated by equation (5): The R_t and R'_t are the charge-transfer resistance values without and with inhibitor respectively. The impedance parameters derived from these investigations are mentioned in Table 4.

$$E_{R_t} \% = \frac{R'_t - R_t}{R_t} \times 100 \quad (4)$$

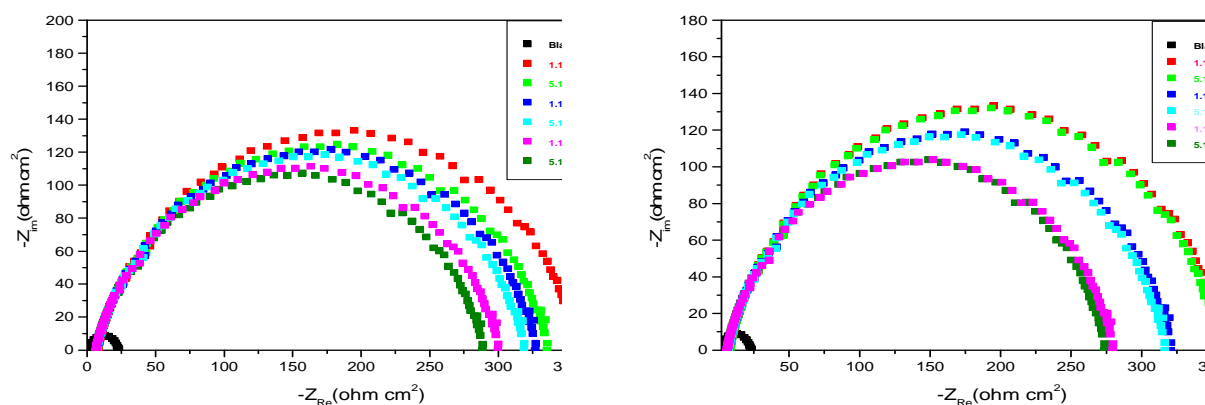


Fig. 3: Nyquist plots of steel in 1M HCl containing various concentration of inhibitor AB8 and AB9 .

From the impedance data (Table 4), we conclude that the value of R_t increases with increase in concentration of the inhibitors and this indicates an increase in the corrosion inhibition efficiency, what is in concord with the gravimetric and electrochemical results obtained. In acidic solution, the impedance diagrams show perfect semi-circles (Fig. 3) whose size increases with the concentration of the inhibitor indicating a charge-transfer process mainly controlling the corrosion of steel. Similar diagrams were described in the literature for the electrode of iron and steel with and without inhibitor 1M HCl [1; 27; 28].

Table 4: Impedance parameters of steel in 1M HCl in the absence and presence of different concentrations of AB8 and AB9 at 308 K

Inhibitor	Concentration (M)	R_t ($\Omega \cdot \text{cm}^2$)	f_{max} (Hz)	C_{dl} ($\mu\text{F}/\text{cm}^2$)	E_{Ri} (%)
1M HCl	0	22.63	55.372	$1.27 \cdot 10^{-4}$	----
AB8	$1 \cdot 10^{-3}$	480,67	7,5123	$9,71 \cdot 10^{-5}$	96
	$5 \cdot 10^{-4}$	360,50	7,5123	$2,41 \cdot 10^{-4}$	94
	$1 \cdot 10^{-4}$	144,20	7,5123	$5,21 \cdot 10^{-5}$	85
	$5 \cdot 10^{-5}$	108,15	8,307	$3,51 \cdot 10^{-5}$	80
	$1 \cdot 10^{-5}$	80,11	8,307	$5,51 \cdot 10^{-5}$	73
	$5 \cdot 10^{-6}$	77,25	8,307	$5,72 \cdot 10^{-5}$	72
AB9	$1 \cdot 10^{-3}$	432,60	7,724	$2,40 \cdot 10^{-5}$	95
	$5 \cdot 10^{-4}$	180,25	7,724	$9,29 \cdot 10^{-5}$	88
	$1 \cdot 10^{-4}$	166,38	7,724	$2,31 \cdot 10^{-4}$	87
	$5 \cdot 10^{-5}$	127,23	11,457	$6,85 \cdot 10^{-5}$	83
	$1 \cdot 10^{-5}$	108,15	11,457	$6,72 \cdot 10^{-5}$	80
	$5 \cdot 10^{-6}$	90,12	7,724	$4,70 \cdot 10^{-5}$	76

In fact, the presence of both inhibitors enhances the value of R_t in acidic solution. Values of double layer capacitance are also brought down to the maximum extent in the presence of inhibitor and the decrease in the values of C_{dl} follows the order similar to that obtained for I_{corr} in this study. The decrease in C_{dl} is due to the adsorption of this compound on the metal surface leading to the formation of film from acidic solution [34].

3.4. Effect of temperature:

In general, corrosion rates increase with increasing temperature. In seawater, this increase is much less than the doubling of reaction rates with each 18°F rise in temperature that would be expected if the reactions were under diffusion control as are many other chemical reactions. For many materials, such as steels, where the oxygen content of the water directly affects the corrosion rate, the effect of temperature is minimal as in situations where the corrosion rate would be increased by increased temperature, the solubility of oxygen is decreased with increasing temperatures and the two effects counteract each other. Steels and iron alloys are particularly insensitive to temperature effects in normal marine immersion. For other alloys that depend on a passive film for their corrosion resistance, the effects of temperature can be more pronounced. At elevated temperatures the solubility oxygen required for repairing protective oxide films found on many passive materials is reduced and the reactions that cause the films to break down are enhanced by the increased temperatures. Many stainless steels have what is essentially a “critical pitting temperature” in seawater that is in the range of temperatures experienced in natural seawater. In cold waters they do not pit but in warmer waters they are susceptible.

For most chemical reactions, the reaction rate increases with increasing temperature. Temperature affects the corrosion rate of metals in electrolytes primary through its effect on factors which control the diffusion rate of

oxygen. The corrosion of iron and steel is an example of this because temperature affects the corrosion rate by virtue of its effect on the oxygen solubility and oxygen diffusion coefficient. As temperature increases the diffusion coefficient of oxygen also increases which tends to increase the corrosion rate. However as temperature is increased oxygen solubility in aqueous solutions decreases until at the boiling point all oxygen is removed; this factor tends to decrease the corrosion rate. The net affect for mild steel, is that the corrosion rate approximately doubles for a temperature rise of 313K up to a maximum temperature at about 343, the rate then falls off in an open system because the decial in oxygen solubility becomes the most important factor. In a closed system, where oxygen cannot escape the corrosion rate continues to increase indefinitely with temperature until all the oxygen is consumed (Source: "Corrosion Control" NAVFAC MO-307 September 1992.)

We have studied the temperature influence on the efficiency of AB8 and AB9. For this purpose, we made weight-loss measurements in the range of temperature 313-333 K, in the absence and presence of inhibitors at 10^{-3} M concentration during 1h of immersion of AB8 and AB9. The corresponding data are shown in Table 5. We remark that the rise in temperature leads to an increase in corrosive rate with and without inhibitor. We also note the increase in the inhibition efficiency of AB8 and AB9 with temperature.

The activation energy can be determined from Arrhenius plots for steel corrosion rate presented in Fig 4. The relation can determine the apparent activation energies :

$$W' = K \exp\left(\frac{-E'_a}{RT}\right)$$

$$W = K \exp\left(\frac{-E_a}{RT}\right)$$
(5)

E_a and E'_a are the apparent activation energies in the absence and presence of inhibitors, respectively. The presence of inhibitor causes a change in the values of apparent activation energy. We remark the slight increase of activation energy in presence of inhibitors as compared to that obtained in the blank. It is obvious that the activation energy of the inhibited solution in this study is increased by increasing the concentration of all inhibitors.

Table 5: Influence of temperature on the corrosion rate of steel immersed in 1M HCl at different concentrations of AB8 and AB9 and the corresponding corrosion inhibition efficiency

Compounds	Concentration (M)	Temperature (K)	W_{Corr} (mg cm ⁻² h ⁻¹)	E_W (%)
HCl	1	308	0,962	--
		313	1,420	--
		323	2,640	--
		333	5,1400	--
AB8	10^{-3}	308	0,090	90,6
		313	0,1620	88,5
		323	0,5810	77,9
		333	1,3100	74,5
AB9	10^{-3}	308	0,0520	94,6
		313	0,2430	82,2
		323	0,6120	76,8
		333	1,2680	75,3

Arrhenius plots for the corrosion rate of mild steel are given in Fig. 4. Values of apparent activation energy of corrosion (E_a) for mild steel in 1 M HCl with the absence and presence of various concentrations of AB8 and AB9 were determined from the slope of $\ln(C_R)$ vs. $1/T$ plots and shown in Table 6.

The value of 55.24 kJ mol⁻¹ obtained for the activation energy E_a of the corrosion process in 1 M HCl lies in the range of the most frequently cited values, the majority of which are grouped around 40 kJ mol⁻¹ [27]. Also, Its can be seen from the Table 6 that the E_a decreased with increasing concentration of AB8 and AB9, but all values of E_a in the range of the studied concentration were higher than those in the absence of AB8 and AB9. The tendency of variation in pre-exponential factor (A) is similar to that in apparent activation energy. The experimental fact that the activation energy is higher in the presence of inhibitor is explained in different ways in literature. According to Riggs and Hurd [27], the decrease in apparent activation energy at higher levels of inhibition arises from a shift of the net corrosion reaction, from one on the uncovered surface to one directly involving the adsorbed sites. This also reveals that the entire process is surface-reaction controlled, since the energy of activation for the corrosion process, both in the absence and presence of inhibitor, was greater than 20 kJ/mol [28]. Szauer et al. explained that the increase in activation energy can be attributed to an appreciable decrease in the adsorption of the inhibitor on the

mild steel surface with increase in temperature [29]. As adsorption decreases more desorption of inhibitor molecules occurs because these two opposite processes are in equilibrium. Due to more desorption of inhibitor molecules at higher temperatures the greater surface area of mild steel comes in contact with aggressive environment, resulting in an increase of corrosion rates with temperature. Using high inhibitor concentrations this problem is avoided, because the coverage degrees are close to saturation. The increase in activation energy after the addition of the inhibitor to the 1 M HCl solution can indicate that physical adsorption (electrostatic) occurs in the first stage [30]. Indeed, AB8 and AB9 molecules are organic bases which are easily protonated to form cationic forms in acid medium. It is logical to assume that in this case the electrostatic cation adsorption is responsible for the good protective properties of this compound. However, the adsorption phenomenon of an organic molecule is not considered only as a physical or as chemical adsorption phenomenon. A wide spectrum of conditions, ranging from the dominance of chemisorptions or electrostatic effects arises from other adsorption experimental data [31].

It is clear that the inhibitive efficiency of the tested AB8 and AB9 decreases with the rise of temperature. This indicates that the compounds are physically adsorbed. Metals and alloys react with hydrochloric acid by giving hydrogen and the metal. The evolved hydrogen is used in reducing hydrochloric acid to various products [29; 30]. Inhibitors protect the metal by adsorbing on to the surface. Hoar showed that inhibitor molecules are adsorbed to a different extent at different types of surface sites and influence the anodic and cathodic reactions unequally [31; 32; 33]. Hoar has further concluded that the adsorption of inhibitor molecules reduces the number of electrode reaction sites and thus inhibition becomes more predominant when the surface is covered with nearly a monolayer of the inhibitor. In AB8 and AB9 molecules, N atom acts as reaction centre leading to the formation of the complex film on the surface of the alloy. The AB8 is an excellent inhibitor it has a polar atoms N and the bromide group in position 3 is a donor group by mesomeric effect, which reinforce the adsorption in the metallic Surface. The cyclic provides a high electron density and it has found that inhibitor efficiency increases with the electron density.

An alternative formulation of the Arrhenius equation is the transition state equation:

$$W = \frac{RT}{Nh} \exp\left(\frac{\Delta S^*}{R}\right) \exp\left(-\frac{\Delta H^*}{RT}\right)$$

(6)

where E_a is the apparent activation corrosion energy, R is the universal gas constant, A is the Arrhenius pre-exponential factor, h is plank's constant, N is Avogrado's number, ΔS_a° is the entropy of activation and ΔH_a° is the enthalpy of activation

A plot of $\ln(W_{\text{corr}}/T)$ vs $1/T$ should give a straight line with a slope of $\Delta H^*/R$ and an intercept of $(\text{Log}(R/Nh) + \Delta S^*/R)$ as shown in Fig 4. From this relation the values of ΔH^* and ΔS^* can be calculated (Table 6). The data show that the thermodynamic parameters (ΔH^* and ΔS^*) of the dissolution reaction of steel in 1M HCl in the presence of the AB8 and AB9 are higher than those of the non-inhibited solution. The positive values of ΔH^* mean that the dissolution process is an exothermic phenomenon and that the dissolution of steel is difficult. Also, the entropy ΔS^* increases negatively with the presence of the inhibitor than the non-inhibited one. This reflects the formation of an ordered stable layer of inhibitor on the steel surface. From the previous data, we can say that Artemisia can be used as an effective inhibitor.

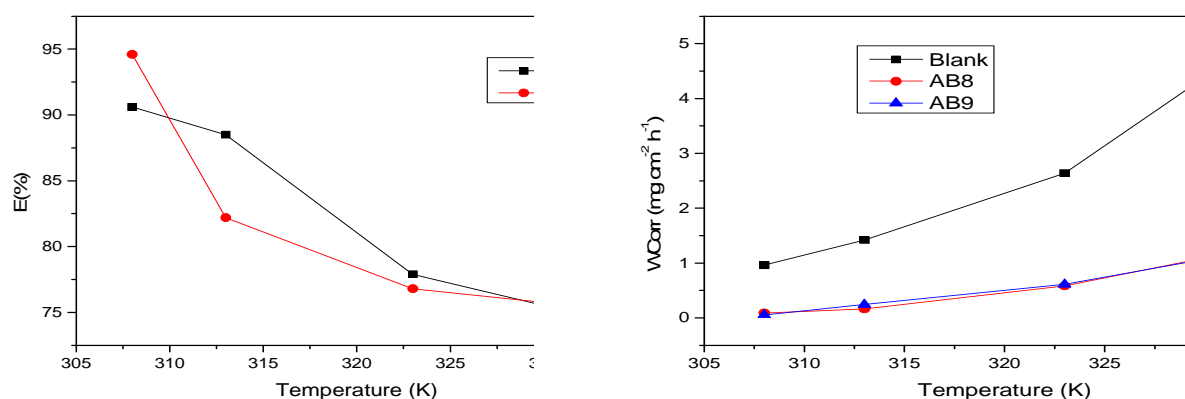


Fig 4.3: Variation E(%) and W as a function of T in 1M HCl with and without 10^{-3} M of AB8 and AB9

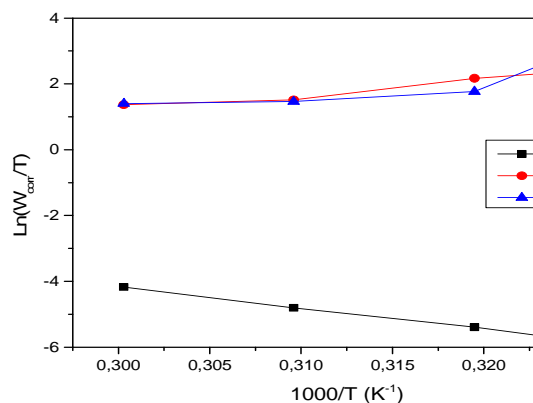


Fig. 4.1 :Variation $\ln W_{\text{corr}}/T$ as a function of $1000/T$ in HCl with and without 10^{-3} M of AB8 and AB9

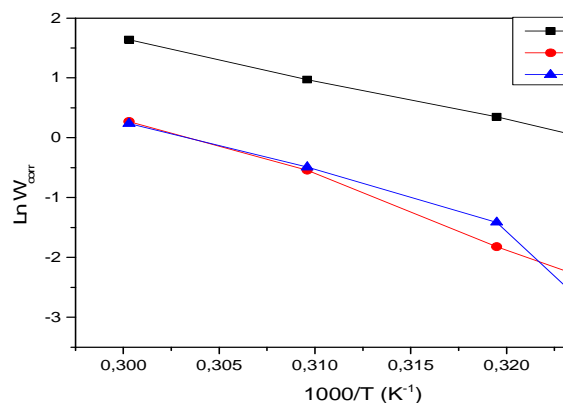


Fig.4.2: Arrhenius plots for the dissolution of steel in 1M HCl in the absence and presence of 10^{-3} M of AB8 and AB9

The positive signs of ΔH_a° reflect the endothermic nature of the mild steel dissolution process suggesting that the dissolution of mild steel is slow [32] in the presence of inhibitor. One can notice that E_a and ΔH_a° values vary in the same way. This result permits to verify the known thermodynamic reaction between the E_a and ΔH_a° as shown in Table 6 [34; 35; 36]:

$$\Delta H_a^\circ = E_a - RT \quad (7)$$

On the other hand, ΔS_a° decreases with increasing AB8 and AB9 concentrations (Table 6) and their values were negative both in the uninhibited and inhibited systems. The negative values of entropies imply that the activated complex in the rate determining step represents an association rather than a dissociation step, meaning that a decrease in disordering takes place on going from reactants to the activated complex [37; 38]. Moreover, ΔS_a° values are more positive in 1 M HCl solutions containing AB8 AND AB9 than that obtained in the uninhibited solution. This behaviour can be explained as a result of the replacement process of water molecules during adsorption of AB8 AND AB9 on the steel surface [35]. This observation is in agreement with the findings of other workers [10; 39].

Table 6: Thermodynamic parameters for steel in different additives of AB8 and AB9

Thermodynamic parameters	Blank	AB8	AB9
E_a (kJ mol ⁻¹)	46.6	91.02	87.2
ΔH_a (kJ mol ⁻¹)	44.9	88.07	84.8
ΔS_a (J mol ⁻¹ K ⁻¹)	-243	-364	-352

3.5. Adsorption isotherm behaviour

Adhesion of atoms, ions, bimolecular or molecules of gas, liquid or dissolved solids to a surface is called adsorption. In this process creates a film of the adsorbate –the molecules or atoms being accumulated, on the surface of the adsorbent In absorption, the molecules of a substance are uniformly distributed in the bulk of the other, whereas in adsorption molecules of one substance are present in higher concentration at the surface of the other substance. Depending upon the nature of forces existing between adsorbate molecules and adsorbent, the adsorption can be classified into two types:

- ✓ Physical adsorption (physisorption): If the force of attraction existing between adsorbate and adsorbent are Vander Waal's forces, the adsorption is called physical adsorption. It is also known as Vander Waal's adsorption. In physical adsorption the force of attraction between the adsorbate and adsorbent are very weak, therefore this type of adsorption can be easily reversed by heating or by decreasing the pressure.
- ✓ 2. Chemical adsorption (chemisorptions): If the force of attraction existing between adsorbate and adsorbent are almost same strength as chemical bonds, the adsorption is called chemical adsorption. It is also known as Langmuir adsorption. In chemisorptions the force of attraction is very strong, therefore adsorption cannot be easily reversed.

The inhibition process is generally related to adsorption of inhibitor's species onto the metallic surface. Then, as illustrated Do, in his reaches, Adsorption equilibrium information is the most important piece of information in understanding an adsorption process. No matter how many components are present in the system, the adsorption equilibrium of pure components are the essential ingredient for the understanding of how much those components can be accommodated by a solid adsorbent.

Various funAB8 and AB9ntal equations are shown, and to start with the proceeding we will present the most basic theory in adsorption: the Langmuir theory (1918). This theory allows us to understand the monolayer surface adsorption on an ideal surface. By an ideal surface here, we mean that the energy fluctuation on this surface is periodic (Fig 5) and the magnitude of this fluctuation is larger than the thermal energy of a molecule (kT), and hence the troughs of the energy fluctuation are acting as the adsorption sites. If the distance between the two neighboring troughs is much larger than the diameter of the adsorbate molecule, the adsorption process is called localised and each adsorbate molecule will occupy one site. Also, the depth of all troughs of the ideal surface are the same, that is the adsorption heat released upon adsorption on each site is the same no matter what the loading is [19; 40; 41]. The Langmuir adsorption isotherm may be written in the following equation (8), where C is the concentration of inhibitor, K is the adsorptive equilibrium constant, θ is the surface coverage and the standard adsorption free energy (ΔG_{ads}°)

$$\frac{C}{\theta} = \frac{1}{K} + C \quad (8)$$

$$\text{with } K = \frac{1}{55.5} \exp\left(-\frac{\Delta G_{ads}^{\circ}}{RT}\right) \quad (9)$$

Langmuir isotherm can also be derived using statistical mechanics with the following assumptions:

- Suppose there are M active sites to which N particles bind.
- An active site can be occupied only by one particle.
- Active sites are independent. Probability of one site being occupied is not dependent on the status of adjacent sites.

The relationship between C/θ and C presents linear behaviour at all temperatures studied (Fig. 4 and 5) with slopes equal to unity.

All the obtained thermodynamic parameters are shown in Table 6. The negative values of ΔG_{ads}° for P1 indicate the spontaneity of the adsorption of P1 and stability of the adsorbed layer on the steel surface. More negative value designates that inhibitor is strongly adsorbed on the steel surface. The negative values of ΔH_{ads}° also show that the adsorption of inhibitor is an exothermic process [1; 2; 4]. It is assumed that an exothermic process is attributed to either physical or chemical adsorption but endothermic process corresponds solely to chemisorptions. In an exothermic process, physisorption is distinguished from chemisorptions by considering the absolute value of a physisorption process is lower than 20 kJ mol^{-1} while the adsorption heat of a chemisorptions process approaches 100 kJ mol^{-1} .

The relationship between C/θ and C presents linear behaviour at all temperatures studied (Fig. 5) with slopes equal to unity. This suggests that the adsorption of AB8 and AB9 on metal surface followed the Langmuir adsorption isotherm (Fig. 5). From the intercepts of the straight lines C_{inh}/θ -axis, the slope is 1.100685 and 1.06407, the intercept is $5.28644 \cdot 10^{-6}$ and $5.83671 \cdot 10^{-6}$ and $K=189163.2175906$ and $K=171329.3961$ respectively for AB8 and AB9. The standard free energy of adsorption values were calculated $\Delta G_{ads}^{\circ} = -41,4282 \text{ Kcal/mol}$ and 57.7143

Kcal/mol respectively for AB8 and AB9. The large negative values of ΔG_{ads}° ensure the spontaneity of the adsorption process and the stability of the adsorbed layer on the mild steel surface as well as a strong interaction between the AB8 and AB9 molecules and the metal surface [42]. This value indicates also that inhibitor interacts on the steel surface by electrostatic effect. These results indicate that the presence of AB8 and AB9 increases the inhibition efficiency without change in adsorption mechanism. The results suggest that the experimental data are well described by Langmuir isotherm.

3.6. Quantum chemical study:

Geometry optimization is a name for the procedure that attempts to find the configuration of minimum energy of the molecule. The procedure calculates the wave function and the energy at a starting geometry and then proceeds to search a new geometry of a lower energy. This is repeated until the lowest energy geometry is found. The procedure calculates the force on each atom by evaluating the gradient (first derivative) of the energy with respect to atomic positions. Sophisticated algorithms are then used at each step to select a new geometry, aiming for rapid convergence to the geometry of the lowest energy. In the final, minimum energy geometry the force on each atom is zero. It is important to recognize that this procedure will not necessarily find the global minimum, i.e. the geometry with the lowest energy. By its nature, a successive search for a minimum finds a local minimum but not necessarily the lowest. In fact, the optimization procedure stops when it finds a stationary point, i.e. a point where forces on the atoms are zero, and this may be also a saddle point (i.e. a transition structure). This will occur particularly if we restrict the symmetry of the molecule and do not allow the program to search the full space of molecular

configurationally degrees of freedom. It is always a good idea to start a procedure of a geometry optimization calculation with a small basis set and a relatively poor method before we move to the basis set and method of choice for a particular problem. You can then start the final geometry optimization from the geometry selected by the simpler and less accurate approach. We can even use the second derivatives of the energy with respect to atomic coordinates (obtained during the optimization process or from a frequency run to further improve the geometry optimization [1; 10] .

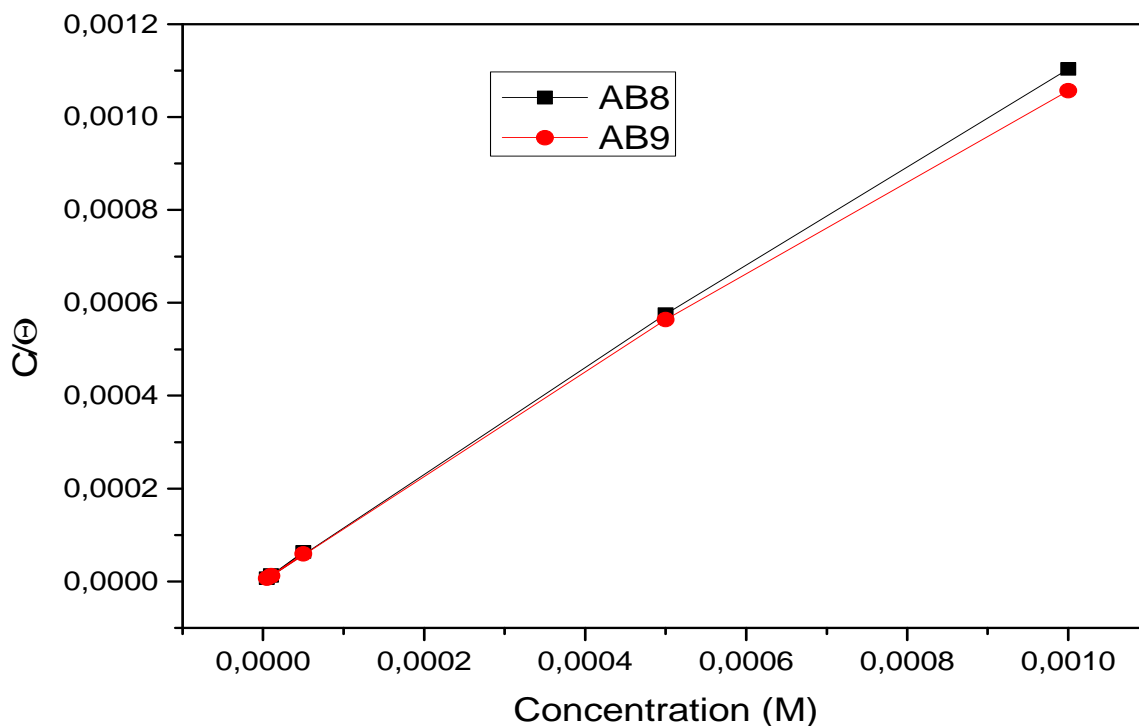


Fig.5. Langmuir isotherm adsorption model of AB 8 and AB9 on the surface of steel in 1M HCl

Complete geometrical optimizations of the investigated molecules are performed using DFT (density functional theory) with the Beck's three parameter exchange functional along with the Lee–Yang–Parr nonlocal correlation functional (B3LYP) [12–14] with 6- 31G* basis set is implemented in Gaussian 03 program package [15]. This approach is shown to yield favourable geometries for a wide variety of systems. This basis set gives good geometry optimizations. The geometry structure was optimized under no constraint. The following quantum chemical parameters were calculated from the obtained optimized structure: several quantum parameters will be determined for possible relations with the inhibitor efficiencies of the pyrazolic molecules (Table 7 and 8) [16; 43].

The energy of HOMO is often associated with the electron donating ability of a molecule. The less negative HOMO energy and the smaller energy gap ($\Delta E = E_{LUMO} - E_{HOMO}$) are often interpreted by a stronger chemisorptions bond and perhaps greater inhibitor efficiency. The calculations were carried out for the pyrazolic derivatives. The geometry of all compounds under investigation was determined by optimizing all geometrical variables without any symmetry constraints. The harmonic frequencies were computed from analytical derivatives for all species in order to define the minimum-energy structures. According to DFT Method, the ionization potential, I can be approximated as the negative of the highest occupied molecular orbital (HOMO) energy [18; 44] ,

$$I = -E_{HOMO} \quad (2) \quad (10)$$

The negative of the lowest unoccupied molecular orbital (LUMO) energy is similarly related to the electron affinity A, In modern terms, we relate affinity to the phenomenon whereby certain atoms or molecules have the tendency to aggregate or bond.

$$A = -E_{LUMO} \quad (3) \quad (11)$$

The electron donating power of a donor molecule is measured by its ionization potential which is the energy required to remove an electron from the highest occupied molecular orbital. The overall energy balance (ΔE), i.e., energy gained or lost, in an electron donor-acceptor transfer is determined by the difference between the acceptor's electron affinity (A) and the ionization potential (I):

$$\Delta E = A - I \quad (12)$$

In chemistry, the class of electron donors that donate not just one, but a set of two paired electrons that form a covalent bond with an electron acceptor molecule, is known as a Lewis base. This phenomenon gives rise to the wide field of Lewis acid-base chemistry. The driving forces for electron donor and acceptor behaviour in chemistry are based on the concepts of electro positivity (for donors) and electronegativity (for acceptors) of atomic or molecular entities. Natural bond orbital (NBO) analysis was performed to evaluate the electron-density distributions. The electron density plays an important role in calculating the chemical reactivity parameters. The global reactivity includes electronegativity, which is identified in the finite difference approximation as the negative of the chemical potential. The ionization energy is typically specified in electron_volts (eV) and refers to the energy required to remove a single electron from a single atom or molecule

$$\chi = \frac{I + A}{2} \quad (13)$$

In 1983 Pearson together with Robert Parr extended the qualitative HSAB theory with a quantitative definition of the **chemical hardness** (η) as being proportional to the second derivative of the total energy of a chemical system with respect to changes in the number of electrons at a fixed nuclear environment :

$$\eta = 1/2 \left(\frac{\partial^2 E}{\partial^2 N} \right)_Z \quad (14)$$

The factor of one-half is arbitrary and often dropped as Pearson has noted. . An operational definition for the chemical hardness is obtained by applying a three-point finite difference approximation to the second derivative :

$$\begin{aligned} \eta &\approx \frac{E(N+1) - 2E(N) + E(N-1)}{2} = \frac{(E(N-1) - E(N)) - (E(N) - E(N+1))}{2}, \\ &= \frac{1}{2}(I - A) \end{aligned} \quad (15a)$$

the global hardness (η) defined as

$$\eta = \frac{I - A}{2} \quad (15b)$$

where I is the ionization potential and A the electron affinity. This expression implies that the chemical hardness is proportional to the band gap of a chemical system, when a gap exists.

The first derivative of the energy with respect to the number of electrons is equal to the chemical potential, μ , of the system,

$$\mu = \left(\frac{\partial E}{\partial N} \right)_Z \quad (16)$$

from which an operational definition for the chemical potential is obtained from a finite difference approximation to the first order derivative as

$$\begin{aligned} \mu &\approx \frac{E(N+1) - E(N-1)}{2}, = \frac{-(E(N-1) - E(N)) - (E(N) - E(N+1))}{2}, \\ &= -\frac{1}{2}(I + A) \end{aligned} \quad (17)$$

which is equal to the negative of the electronegativity (χ) definition on the Mulliken scale: $\mu = -\chi$. The hardness and Mulliken electronegativity are related as:

$$2\eta = \left(\frac{\partial \mu}{\partial N} \right)_Z \approx -\left(\frac{\partial \chi}{\partial N} \right)_Z \quad (18)$$

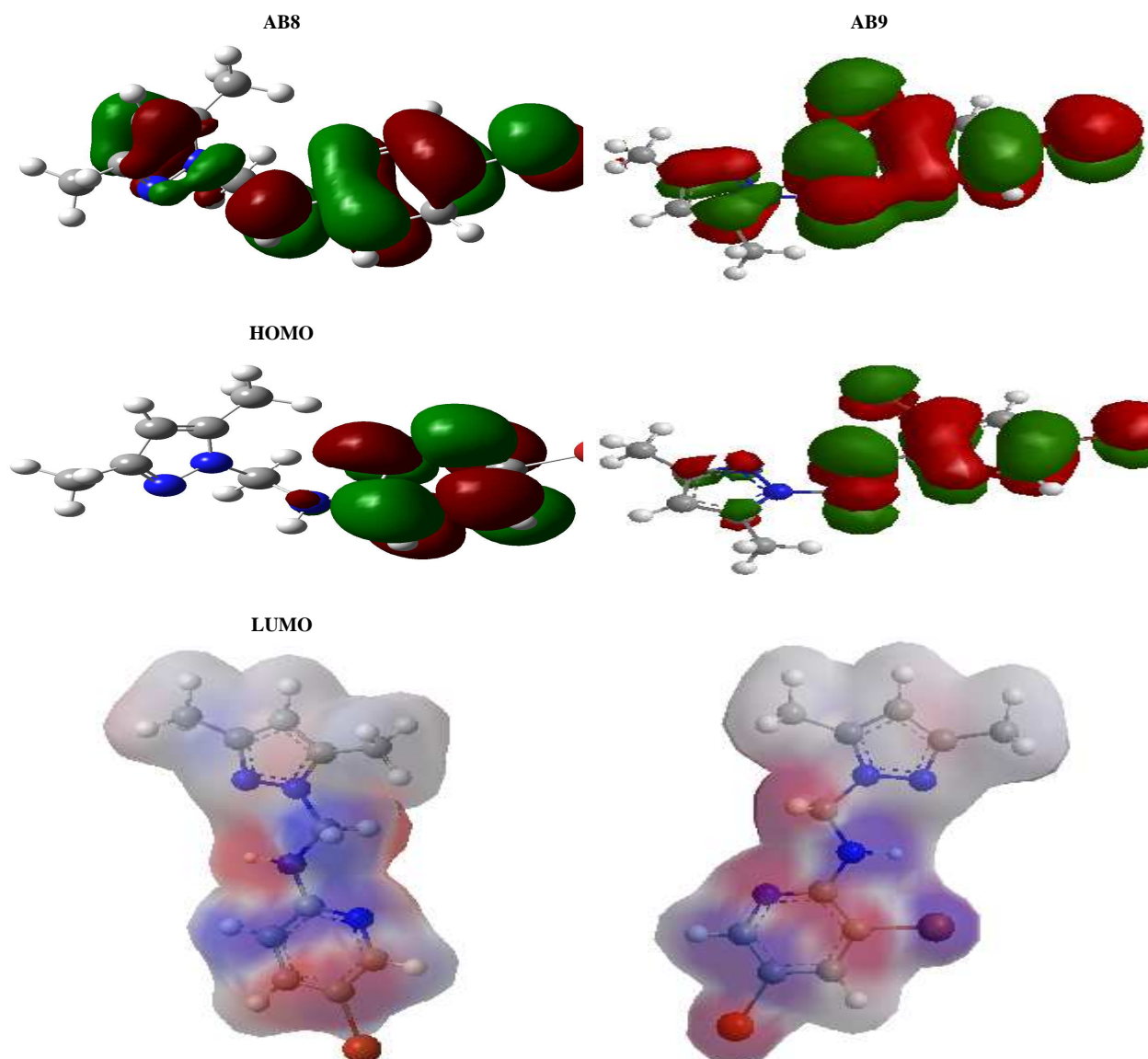
and in this sense hardness is a measure for resistance to deformation or change. Likewise a value of zero denotes maximum **softness**, where softness is defined as the reciprocal of hardness. and the global softness (σ) as its inverse:

$$\sigma = \frac{1}{\eta} \quad (19)$$

During the interaction of the pyrazolic derivatives with the steel surface, electrons flow from the lower electronegativity pyrazolic derivative to the higher electronegativity steel surface until the chemical potential becomes equalized. The fraction of the transferred electron, ΔN was estimated according to Pearson [18; 45]:

$$\Delta N = \frac{\chi_{Fe} - \chi_{inh}}{2(\eta_{Fe} - \eta_{inh})} \quad (20)$$

Quantum chemical parameters obtained from the calculations which are responsible for the inhibition efficiency of inhibitors, such as the highest occupied molecular orbital (E_{HOMO}), energy of lowest unoccupied molecular orbital (E_{LUMO}), HOMO–LUMO energy gap (ΔE_{H-L}), dipole moment (μ) and total energy (TE), electronegativity (χ), electron affinity (A), global hardness (η), softness (σ), ionization potential (I), The global electrophilicity (ω), the fraction of electrons transferred from the inhibitor to steel surface (ΔN) and the total energy (TE), are collected in Table 7 and 8



TCD

Fig 6 : HOMO, LUMO and total charge density (TCD) of AB8 and AB9 respectively

In Fig. 6, we have presented the frontier molecule orbital density distributions of the studied compounds. Analysis of Fig. 6 shows that the distribution of two energies HOMO and LUMO, we can see that the electron density of the HOMO location in the pyrazolic molecules is mostly distributed near the nitrogen (N) atoms and pyridine rings indicating that these are the favourite sites for adsorption, while the density LUMO was distributed almost of the entire molecules.

The E_{HOMO} is a quantum chemical parameter which is often associated with the electron donating ability of the molecule. High value of $E_{\text{HOMO}} = -0.21415$ eV for AB9 is likely to a tendency of the molecule to donate electrons to appropriate acceptor molecule of low empty molecular orbital energy and indicates also the better inhibition efficiency [16]. It has also been found that an inhibitor does not only donate an electron to the unoccupied d orbital of the metal ion but can also accept electrons from the d orbital of the metal leading to the formation of a feedback bond. Therefore, the tendency for the formation of a feedback bond would depend on the value of E_{LUMO} . The lower the E_{LUMO} , the easier is the acceptance of electrons from the d orbital of the metal. Based on the values of E_{LUMO} , the order obtained for the decrease in inhibition efficiency ($\text{AB9} < \text{AB8}$) was also similar to the one obtained from experimental results.

Table 7. Partial total atomic charges calculated and quantum parameters.

Inhibitor	N(2)	N(3)	N(9)	N(15)	C(5)	E_{LUMO} (eV)	E_{HOMO} (eV)	ΔE (eV)
AB8	-0.51508	-0.28025	-0.65625	-0.45235	-0.25330	-0.03504	-0.21777	-0.18273
AB9	-0.57446	-0.28023	-0.73593	-0.45100	-0.24600	-0.03660	-0.21415	-0.17775
	C(6)	C(7)	C(11)	C(12)	C(13)	μ (Debye)	E_{HF} (a.u)	Mol. Volume (bohr ³ /mol)
AB8	-0.48115	-0.45853	-0.10925	-0.08584	-0.29905	0.7483	-3217.38657	1663.937
AB9	-0.47247	-0.45835	-0.30194	-0.06445	-0.29509	3.4357	-5788.35543	2422.268

A band gap, also called an energy gap or band gap, is an energy range in a solid where no electron states can exist. In graphs of the electronic band structure, the band gap generally refers to the energy difference (in electron volts) between the top of the valence band and the bottom of the conduction band in metal. This is equivalent to the energy required to free an outer shell electron from its orbit about the nucleus to become a mobile charge carrier, able to move freely within the solid material, so the band gap is a major factor determining the electrical conductivity of a metal.

We concluded that the large values of the energy gap (ΔE) imply high electronic stability and then low reactivity, when low values imply that it will be easier to remove an electron from the HOMO orbital to LOMO one which can result in good inhibition efficiency. As ΔE decreases, the reactivity of the molecule increases leading to increase the inhibition efficiency of the molecule.

The results presented in Table 7 show that $\Delta E_{\text{gap}} = E_{\text{LUMO}} - E_{\text{HOMO}} = 0.17775$ eV for AB9 have the lowest energy gaps. Therefore, their higher reactivity can allowed them to be easily adsorbed onto the mild steel surface leading to increase their inhibitive efficiencies compared to AB8 $\Delta E_{\text{gap}} = 0.18273$ eV [46].

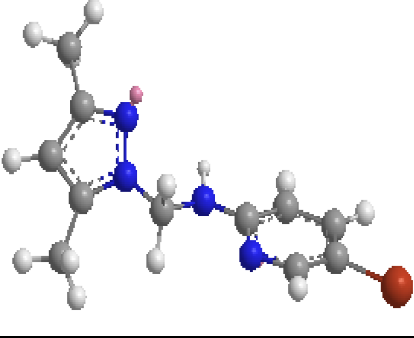
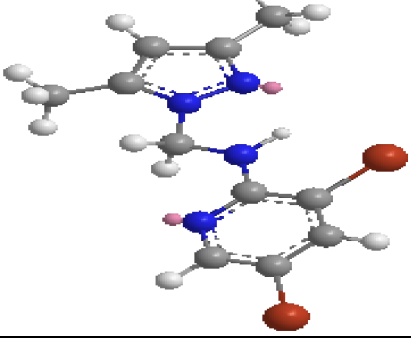
Dipole moment is the measure of polarity of a polar covalent bond. It is defined as the product of charge on the atoms and the distance between the two bonded atoms. The dipole moment of the molecule gives information on the polarity of the given system, however, reflects only the global polarity of a molecule. For a complete molecule the total molecular dipole moment may be approximated as the vector sum of individual bond dipole moments.

The dipole moment (μ in Debye) is another important electronic parameter that results from non uniform distribution of charges on the various atoms in the molecule. Molecules that have high dipole moment have a tendency to interact with other molecule through electrostatic interactions (e.g., dipole-dipole interactions). The high value of dipole moment probably increases the adsorption between chemical compound and metal surface [43; 46]. The energy of the deformability increases with the increase in μ , making the molecule easier to adsorb at the steel surface. The volume of the inhibitor molecules also increases with the increase of μ . This increases the contact area between the molecule and surface of steel and increasing the corrosion inhibition ability of inhibitors.

The dipole moment of a molecule is strongly determined by the shape of the molecule, size of the molecule and type of atoms constituting the molecule. The relationship between inhibition efficiencies and dipole moment of similar molecules have often given results that are not univocal, i.e., in some instances the dipole moment appears to increase with increasing inhibition efficiencies, while in other systems the dipole moment appears to decrease with increase in the inhibition efficiencies of the inhibitors. In our study, there is direct relationship between the $E_{\text{I}}(\%)$ and the dipole moment The results of the dipole moment for the AB8 and AB9 are reported in Table 7. The dipole

moment follows the order; $\mu=3.4357$ Debye for AB9 > $\mu=0.7483$ Debye for AB8, which is not in agreement with trends in the experimental inhibition efficiencies of the inhibitors earlier reported in literature [47].

Table 8: Quantum Parameters for AB8 and AB9

Structure Minimization by MM2 method		
Quantum parameters	AB8	AB9
Dipole/Dipole	0.2841	0.3610
Stretch	12.6827	12.6918
Bend	-0.1418	-0.1139
Stretch-Bend	-1.6726	-0.3788
Torsion	-2.7424	-3.6641
Non-1,4 VDW	4.8951	5.9160
1,4 VDW	-2.6659	-0.3734
E_{HOMO} (eV)	-0.21777	-0.21415
E_{LUMO} (eV)	-0.03504	-0.03660
ΔE gap (eV)	0.18273	0.17775
μ (Debye)	0.7483	3.4357
$I = -E_{HOMO}$ (eV)	0.21777	0.21415
$A = -E_{LUMO}$ (eV)	0.03504	0.03660
$\chi = \frac{I + A}{2}$ (eV)	0.126405	0.125375
$\eta = \frac{I - A}{2}$ (eV)	0.091365	0.088775
$\sigma = \frac{1}{\eta}$	10.9451	11.2644
$\omega = \frac{\mu^2}{2\eta}$	3.06437	66.4828
$\Delta N = \frac{\chi_{Fe} - \chi_{inh}}{2(\eta_{Fe} - \eta_{inh})}$	-37.6161	3.8718

The total energy presented in the table 7, calculated by quantum chemical methods is also a beneficial parameter. The total energy of a system is composed of the internal, potential, and kinetic energy. The total energy of a system including that of the many body effects of electrons (exchange and correlation) in the presence of static external potential (for example, the atomic nuclei) is a unique functional of the charge density. The minimum value of the total energy functional is the ground state energy of the system. The electronic charge density which yields this minimum is then the exact single particle ground state energy. In our study the total energy of the best inhibitor AB9 is equal to -5788.355431 a.u., this value is lower than that of the compound AB8 is equal to 3217.386571 a.u.

Mulliken charges showed in table 7, arise from the Mulliken population analysis and provide a means of estimating partial atomic charges from calculations carried out by the methods of computational chemistry, particularly those based on the linear combination of atomic orbital molecular orbital method. The Mulliken charges obtained using DFT/B3LYP/6-31G is significantly different from the results of other methods. This result is consistent with the fact that Mulliken atomic charges are strongly basis-set sensitive and in most instances tend to become unphysical when large basis sets with diffuse functions are employed. The Mulliken atomic charges obtained are also not realistic. The partial charges on the individual atoms in a molecule also indicate the reactive

centres for a particular inhibitor. Atoms with the highest negative charge are considered to have an electron donor role when interacting with metal surfaces. The Mulliken atomic charges for the heteroatom's of the pyrazolic derivatives are reported in table 7 and show that N atoms has the highest negative charge. The partial charges on the individual atoms in a molecule also indicate the reactive centres for a particular inhibitor. Atoms with the highest negative charge are considered to have an electron donor role when interacting with metal surfaces. Moreover, the negative charge on the N atom increases across the structures following the order; AB9>AB8 for example the N(9) charge is -0.735938 eV and -0.656250 respectively for AB9 and AB8 .

This result is consistent with the fact that the electron withdrawing effect of the Bromide in position 3 and 3,5 for AB8 and AB9 respectively, decreases the negative charge on the N atom in the ring while the electron donating role. In view of the above results, AB9 has greater tendency to adsorb on the metal surface because it has three highly negative charged centres while AB8 is preferentially the molecule with the least negative charge.

Absolute hardness and softness are important properties to measure the molecular stability and reactivity. It is apparent that the chemical hardness fundamentally signifies the resistance towards the deformation or polarization of the electron cloud of the atoms, ions or molecules under small perturbation of chemical reaction. A hard molecule has a large energy gap and a soft molecule has a small energy gap [19; 43]. Soft molecules are more reactive than hardness because they can easily offer electrons. Hence, inhibitors with the highest values of global softness (the least values of the global hardness) are expected to be good corrosion inhibitors for bulk metals in acidic media. For the simplest transfer of electron, adsorption could occur at the part of the molecule where softness (σ), which is a local property, has a highest value. In our present study AB9 with low softness value $\sigma = 11.2644$ (eV) compared with other compound have a low energy gap. The most widely used quantity to describe the polarity is the dipole moment of the molecule.

The fraction of electrons transferred describes the trend of electrons donation within a set of inhibitors. In literature it has been reported that the values of ΔN show inhibition effect resulted from electrons donation. According to study, the inhibition efficiency increased with increasing electron donating ability of inhibitor at the metal surface and increasing electron-donating ability at the metal surface.. Also it was observed that inhibition efficiency increased with increase in the values of ΔN . The obtained values of ΔN reported in Table 8, the AB9 has higher values of $\Delta N=3.8718$ eV than AB8. This result implies good disposition of AB9 molecules to donate their electrons leading to increase their adsorption on the metal surface and to increase their inhibition efficiencies [43].

It is worth noting that all the computed descriptors are in total agreement with the experimental inhibition efficiencies of the investigated inhibitors, presented in Table 8 which confirm that the presence of Br atoms in position 3,5 and 3 for AB9 and AB8 enhance the donor abilities of these molecules increasing their adsorption on the metal surface and thereby leading to higher experimental inhibition efficiencies.

CONCLUSION

The principal finding of the present work can be summarised as follows:

- The results obtained showed the effectiveness of the investigated pyrazolic deriviers as a good inhibitor of mild steel in 1 M HCl.
- The pyrazolic inhibitors act a mixed inhibitor without modifying the hydrogen reduction mechanism.
- The adsorption of the AB8 and AB9 on the steel surface in 1M HCl obeys to the Langmuir adsorption isotherm model.
- The inhibition efficiency of all inhibitors increases with the temperature and the activation corrosion energy decreases in presence of inhibitor.
- Quantum chemical studies have been performed, using the B3LYP/6-31G method to investigate the properties of AB8 and AB9 and how their molecular properties relate to their ability to inhibit metal corrosion. The calculated electronic parameters involved in the activity of the inhibitors. A comparison of all the molecular properties suggests that AB9 is a better corrosion inhibitor than AB8.

Acknowledgment

The authors want to thank the CUD of Belgium and CNRST (Morocco) for their generous support.

REFERENCES

- [1] I Belfilali, A Chetouani, B Hammouti, A Aouniti, S Louhibi, and SS Al-Deyab *International Journal of Electrochemical Science*, 2012, 7, 3997-4013

- [2] A Sirajunnisa, M I Fazal Mohamed and A Subramania, *Journal of Chemical and Pharmaceutical Research*, **2014**, 6(1), 580-588
- [3] A Chetouani, K Medjahed, SS Al-Deyab, B Hammouti, I Warad, A Mansri, and A Aouniti, *International Journal of Electrochemical Science*, **2012**, 7, 6025-6043
- [4] M Ferhat, A Benchettara, SE Amara, D Najjar, *J Mater Environ Sci* **2014**, 5 (4), 1059-1068
- [5] M Abdallah, I Zaafrany, KS Khairou, and Y Emad, *Chemistry and Technology of Fuels and Oils*, **2012**, 48, 234-245
- [6] A Ghazoui, A Zarrouk, N Benaft, R Salghi, M Assouag, M El Hezzat, A Guenbour and B Hammouti, *Journal of Chemical and Pharmaceutical Research*, **2014**, 6(2), 704-712
- [7] F Bentiss, M Outirite, M Traisnel, H Vezin, M Lagrenee, B Hammouti, SS Al-Deyab, and C Jama, *International Journal of Electrochemical Science*, **2012**, 7, 1699-1723
- [8] H Zarrok, A Zarrouk, B Hammouti, R Salghi, C Jama, and F Bentiss, *Corrosion Science*, **2012**, 64, 243-252
- [9] KF Khaled, NS Abdel-Shafi, *J Mater Environ Sci* **2014**, 5 (4), 1288-1297
- [10] MJ Firdhouse, and D Nalini, *Journal of Chemistry*, **2013**
- [11] M Boudalia, A Bellaouchou, A Guenbour, H Bourazmi, M Tabiyaoui, M El Fal, Y Ramli, H Elmsellem *Mor J Chem* **2014**, 2(2), 97-109
- [12] HTM Abdel-Fatah, *Anti-Corrosion Methods and Materials*, **2012**, 59, 23-31
- [13] K Bouhrira, F Ouahiba, D Zerouali, B Hammouti, M Zertoubi, and N Benchat, *E-Journal of Chemistry*, **2010**, 7, S35-S42
- [14] MH Majeed, A A Sultan and HH Al-Sahlane, *Journal of Chemical and Pharmaceutical Research*, **2014**, 6(5), 996-1001
- [15] A Chetouani, H Elmsellem, H Bendaha, A Aouniti, M Mimouni, A Bouyanzer, *Mor J Chem* **2014**, 2(1), 1-9
- [16] N Boussalah, S Ghalem, S El Kadiri, B Hammouti, and R Touzani, *Research on Chemical Intermediates*, **2012**, 38, 2009-2023
- [17] Z El Adnani, M McHarfi, M Sfaira, M Benzakour, AT Benjelloun, and M Ebn Touhami, *Corrosion Science*, **2013**, 68, 223-230
- [18] EE Ebenso, MM Kabanda, T Arslan, M Saracoglu, F Kandemirli, LC Murulana, AK Singh, SK Shukla, B Hammouti, KF Khaled, MA Quraishi, IB Obot, and NO Eddy, *International Journal of Electrochemical Science*, **2012**, 7, 5643-5676
- [19] H Zarrok, SS Al-Deyab, A Zarrouk, R Salghi, B Hammouti, H Oudda, M Bouachrine, and F Bentiss, **2012**, 7, 4047-4063
- [20] G Gao, and CH Liang, *Electrochimica Acta*, **2007**, 52, 4554-4559
- [21] S Chen, and T Kar, *International Journal of Electrochemical Science*, **2012**, 7, 6265-6275
- [22] J Xu, XQ Wu, and EH Han, *Electrochimica Acta*, **2012**, 71, 219-226
- [23] TY Namoussa, S Ladjel, N Gherraf, MR Ouahrani, *J Chem Pharm Res*, **2010**, 2(4), 808-811
- [24] K Lau, and A Sagues, *Electrochimica Acta*, **2011**, 56, 7815-7824
- [25] V HorvatRadosevic, and K Kvastek, *Electrochimica Acta*, **1997**, 42, 1403-1419
- [26] SK Poznyak, AD Lisenkov, MGS Ferreira, AI Kulak, and ML Zheludkevich, *Electrochimica Acta*, **2012**, 76, 453-461
- [27] M Kaddouri, M Bouklah, S Rekkab, R Touzani, SS Al-Deyab, B Hammouti, A Aouniti, and Z Kabouche, *International Journal of Electrochemical Science*, **2012**, 7, 9004-9023
- [28] M Zerfaoui, B Hammouti, H Oudda, M Benkaddour, and S Kertit, *Bulletin of Electrochemistry*, **2004**, 20, 433-437
- [29] K Barouni, L Bazzi, R Salghi, M Mihit, B Hammouti, A Albourine, and S El Issami, *Materials Letters*, **2008**, 62, 3325-3327
- [30] M Bouklah, A Attayibat, S Kertit, A Ramdani, and B Hammouti, *Applied Surface Science*, **2005**, 242, 399-406
- [31] AY Musa, AAH Kadhum, MS Takriff, AR Daud, SK Kamarudin, and N Muhamad, *Corrosion Engineering Science and Technology*, **2010**, 45, 163-168
- [32] BG Pound, *Journal of Biomedical Materials Research Part B-Applied Biomaterials*, **2010**, 94B, 287-295
- [33] Ranjana, R Banerjee, and MM Nandi, *Indian Journal of Chemical Technology*, **2010**, 17, 176-180
- [34] D Ben Hmamou, R Salghi, L Bazzi, B Hammouti, SS Al-Deyab, L Bammou, and A Bouyanzer, *International Journal of Electrochemical Science*, **2012**, 7, 1303-1318
- [35] M Dahmani, SS Al-Deyab, A Et-Touhami, B Hammouti, A Bouyanzer, R Salghi, and A ElMejdoubi, *International Journal of Electrochemical Science*, **2012**, 7, 2513-2522
- [36] L Herrag, M Bouklah, NS Patel, BM Mistry, B Hammouti, S Elkadiri, and M Bouachrine, *Research on Chemical Intermediates*, **2012**, 38, 1669-1690
- [37] L Herrag, B Hammouti, S Elkadiri, A Aouniti, C Jama, H Vezin, and F Bentiss, *Corrosion Science*, **2010**, 52, 3042-3051
- [38] P Mohan, R Usha, GP Kalaignan, and VS Muralidharan, *Journal of Chemistry*, **2013**

-
- [39] H Akrouf, L Bousselmi, S Maximovitch, E Triki, and F Dalard, *Journal of Materials Science*, **2012**, 47, 8085-8093
- [40] N Soltani, N Tavakkoli, M Khayatkashani, MR Jalali, and A Mosavizade, *Corrosion Science*, **2012**, 62, 122-135
- [41] W Lai, and F Ciucci, *Electrochimica Acta*, **2010**, 56, 531-542
- [42] A Ouchrif, M Zegmout, B Hammouti, A Dafali, M Benkaddour, A Ramdani, and S Elkadiri, *Progress in Organic Coatings*, **2005**, 53, 292-296
- [43] Y Karzazi, M El Alaoui Belghiti, A Dafali and B Hammouti, *Journal of Chemical and Pharmaceutical Research*, **2014**, 6(4), 689-696
- [44] K Laarej, M Bouachrine, S Radi, S Kertit, and B Hammouti, *E-Journal of Chemistry*, **2010**, 7, 419-424
- [45] NO Obi-Egbedi, IB Obot, and MI El-Khaiary, *Journal of Molecular Structure*, **2011**, 1002, 86-96
- [46] EH El Ashry, A El Nemr, and S Ragab, *Journal of Molecular Modeling*, **2012**, 18, 1173-1188
- [47] W Li, L Hu, Z Tao, H Tian, and B Hou, *Materials and Corrosion-Werkstoffe Und Korrosion*, **2011**, 62, 1042-1050